Pergamon

Int. J. Heat Mass Transfer. Vol. 41, Nos 6–7, pp. 963–974, 1998

Printed in Great Britain
0017-9310/98 $19.00+0.00

PII: S0017-9310(97)00231-7

On the heat balance during double-gated, modulated-pressure injection moulding

T. ZHANG*, J. R. G. EVANS and M. J. BEVIS

Department of Materials Engineering, Brunel University, Uxbridge, Middlesex UB8 3PH, U.K.

(*Received* 21 *September* 1995)

Abstract—Double-gated, modulated-pressure moulding provides orientation of molecules or fibres so that the properties of materials can be controlled during processing. A numerical method for estimating the duration of oscillating flow under a preset pressure amplitude based on the balance of viscous heating and loss to the mould wall is described. This first attempt to quantify an extremely complex process allows the effects of moulding parameters on solidification to be deduced and the experimental array reduced. The predictions are compared with experimental results for high and low thermal diffusivity materials. © 1997 Elsevier Science Ltd.

1. INTRODUCTION

In conventional single-gated injection moulding, particularly of composite materials, there is little opportunity to control orientation throughout a component [1]. If an injection moulding cavity is multigated, it is possible to cause reciprocating flow of the molten contents via selected gates [2, 3]. This allows molecules and anisotropic shaped particles or fibres to be aligned and to be retained in alignment as they are occluded by the solidifying matrix. This method has also been applied to the control of orientation in unfilled semicrystalline polymers [4], liquid crystal polymers [5], metal matrix composites [6] and fibre reinforced extrudates [7].

The heat generated during reciprocating flow prolongs the solidification of both the cavity contents and those of the narrow channels used to feed it. Reciprocating flow can only take place if sufficient pressure acts on the melt and at high pressures a steady state is reached and the internal source of heat allows reciprocation to continue indefinitely. The size of the molten zone depends on the balance of heat generated by viscous flow and heat lost to the mould wall. The principal variables over which the operator has control are modulated pressure amplitude, oscillation frequency, mould temperature and sprue and runner size.

The practical problem, which in the absence of quantitative analysis can be overcome only by expensive tooling changes in trial and error iteration, is that for low thermal diffusivity materials reciprocation can continue indefinitely forbidding orientation control in the core of the moulding while for high thermal diffusivity materials such as metal or ceramic powder suspensions solidification occurs too rapidly in the runners which also forbids control. How should the mould tool configuration be chosen for a given material for a permitted set maximum pressure amplitude and frequency?

2. THEORY

In order to render the analysis of this complicated moulding operation tractable, several assumptions are needed. Their justifications are stated here and where appropriate, justified by perturbation of the model, in Section 5. The moulding flow paths are shown schematically in Fig. 1. Upon mould filling, the initial temperature of the cavity contents was taken as the nozzle temperature. Mould filling took 2–3 s which is comparable to half the cycle time for oscillation defined in Fig. 2. Oscillation commenced automatically after filling so heat flow during filling need not be treated separately. It is only after the prolonged solidification stage when the molten channel diameters are small that the heat balance becomes critical by controlling freezing at some point in the flow path. The pistons (Fig. 1) discharged their entire contents on each cycle. Observation showed that it was only in the few cycles before freeze-off that the pistons failed to discharge in time. The displaced volume is therefore equal to the piston displacement. Heat is lost to the mould wall and the mould temperature was thermostatically controlled so that a convective boundary condition can be used [8]. Heat is also supplied by viscous dissipation in the molten flowing core. Laminar flow was considered in the molten region since Reynolds number was only 6×10^{-4}–9×10^{-2} and the observation that fibres are aligned by the process [2] supports this hypothesis.

Heat is also exchanged between the melt in transit and the nozzle or oscillation cylinder and this may affect the temperature distribution in the rest of the

*Present address; School of Engineering Systems and Design, South Bank University, London, U.K.

NOMENCLATURE

C_1	constant of integration [m s^{-1}]
C_p	specific heat [J kg^{-1} K^{-1}]
h	surface heat transfer coefficient [W m^{-2} K^{-1}]
ΔH_m	enthalpy of melting [J kg^{-1}]
k	thermal conductivity [W m^{-1} K^{-1}]
n	flow behaviour index
P	pressure [Pa]
$\mathbf{q}_r$	heat flux vector [J m^{-2} s^{-1}]
Q	volume flow rate [m^3 s^{-1}]
r	radius [m]
R	radius of the molten channel [m]
t	time [s]
T	temperature [°C]
T_n	temperature of node n [°C]
T_m	mould temperature [°C]
ΔT_m	melting range [°C]
V_z	velocity in the Z direction [m s^{-1}]
x	distance in the rectangular bar section [m]
y	distance in the rectangular bar section [m]
Z	distance in the direction of mass flow [m].

Greek symbols

α	thermal diffusivity [m^2 s^{-1}]
γ	shear rate [s^{-1}]
γ_{rz}	shear stress vector [Pa]
η_0	viscosity constant [Pa s]
ρ	density [kg m^{-3}].

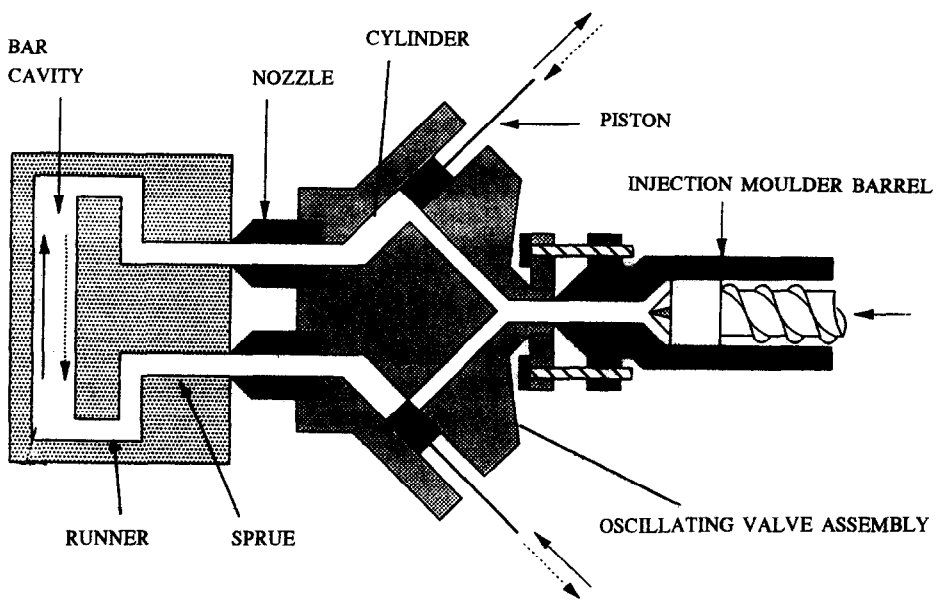

Fig. 1. Schematic diagram of the double-gated reciprocating flow paths.

circuit during oscillation [9]. This effect is explored in Section 5. The analysis for heat dissipated in viscous flow treats the molten zone in the sprue and runners as cylinders and the justification for this is given. It is argued below that heat dissipated by viscous flow in the thick section of the moulding can be neglected by comparison with that dissipated in the sprue and runners because of the lower shear rates therein. The cylinders are long in comparison with their radii and are therefore treated as infinite.

The molten channel, under laminar flow conditions, contains a temperature gradient and hence a viscosity gradient. Fortunately, for polypropylene and other semicrystalline polymers, the viscosity changes very little with temperature above the solidification region as shown experimentally. In the melting region it rises steeply as crystallization commences. Initially therefore, viscosity was treated as constant with temperature but the effect of viscosity was subsequently explored in more detail.

The moulding materials (unfilled polymer and 60 vol% ceramic–polymer suspension) were considered incompressible in the liquid and solid states at the pressures employed ($P \leqslant 165$ MPa). The volume changes associated with the maximum pressure are in the region of 11% and 4% for the polypropylene and

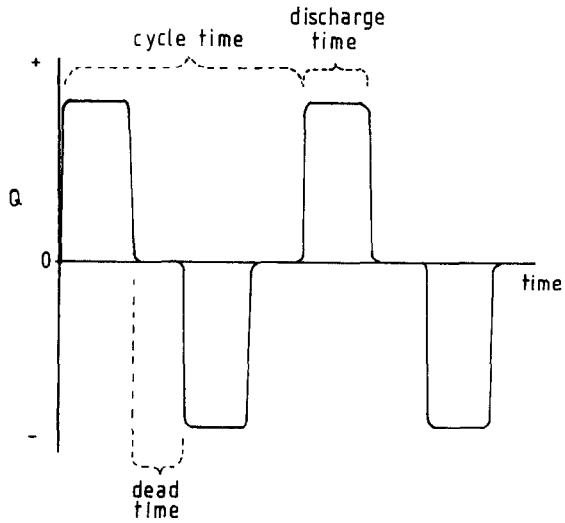

Fig. 2. Schematic diagram of the rate of volumetric displacement.

ceramic composition respectively at 200°C. Since in most cases the maximum pressure was only reached just before flow stopped, the true volume change induced by pressure variation is smaller than these values. Similarly, the viscosity was considered to be independent of pressure. In fact, the viscosity of polymers does increase with pressure [10] and the effect of changing viscosity is explored.

The temperature distribution in the moulded bars during solidification without an internal heat source was calculated by a two dimensional finite difference method. Since the area of the exposed ends was 120 mm^2 compared to the surface area of the sides (2240 mm^2) the heat loss from the ends was neglected.

The general equation for heat transfer from the bar is

$$\frac{\partial^2 T}{\partial x^2}+\frac{\partial^2 T}{\partial y^2}=\frac{1}{\alpha}\frac{\partial T}{\partial t} \tag{1}$$

Likewise without oscillating flow, the heat transfer in a cylinder is sufficiently described by the one dimensional differential equation:

$$\frac{\partial^2 T}{\partial r^2}+\frac{1}{r}\frac{\partial T}{\partial r}=\frac{1}{\alpha}\frac{\partial T}{\partial t} \tag{2}$$

A finite difference method in the explicit form was used to solve eqns (1) and (2) [11] and an energy balance method was used for the boundary node. In a cylindrical channel with laminar flow, the derivatives of temperature, velocity and shear stress with respect to the circumferential and axial directions are zero. Neglecting the initial acceleration of the melt, thus assuming stable flow throughout the discharge, the momentum equation reduces to

$$\frac{\partial P}{\partial Z}=\frac{1}{r}\frac{\partial}{\partial r}(r\tau_{rz}) \tag{3}$$

and the energy equation reduces to

$$\rho C_p\frac{\partial T}{\partial t}=-\frac{1}{r}\frac{\partial}{\partial r}(r\mathbf{q}_r)+\tau_{rz}\left(\frac{\partial V_z}{\partial r}\right) \tag{4}$$

For the material which is flowing, the shear stress is given for a power law fluid by

$$\tau_{rz}=\eta_0\left(\frac{\partial V_z}{\partial r}\right)^n \tag{5}$$

The only non-zero heat flux vector $\mathbf{q}_r$ is given by

$$\mathbf{q}_r=-k\frac{\partial T}{\partial r} \tag{6}$$

Introducing eqn (5) into eqn (3) gives

$$\frac{\partial P}{\partial Z}=\frac{\eta_0}{r}\frac{\partial}{\partial r}\left[r\left(\frac{\partial V_z}{\partial r}\right)^n\right] \tag{7}$$

and integration with respect to r yields

$$r\left(\frac{\partial V_z}{\partial r}\right)^n=\frac{r^2}{2\eta_0}\left(\frac{\partial P}{\partial Z}\right)+C_1 \tag{8}$$

The boundary conditions at the surface and centre of the flowing zone are respectively:

$$V_z=0 \quad \text{at } r=R$$

$$\frac{\partial V_z}{\partial r}=0 \quad \text{at } r=0 \tag{9}$$

giving:

$$\frac{\partial V_z}{\partial r}=\left[\frac{r}{2\eta_0}\left(\frac{\partial P}{\partial Z}\right)\right]^{1/n} \tag{10}$$

or

$$\frac{\partial P}{\partial Z}=\frac{2\eta_0}{r}\left(\frac{\partial V_z}{\partial r}\right)^n \tag{11}$$

Using the Rabinowitsch correction [12] for the wall shear rate ($r=R$):

$$\frac{\partial V_z}{\partial r}=\frac{3n+1}{n}\frac{Q}{\pi R^3} \tag{12}$$

and combining eqns (11) and (12):

$$\frac{\partial P}{\partial Z}=2\left(\frac{3n+1}{n\pi}\right)^n\eta_0\frac{Q^n}{R^{3n+1}} \tag{13}$$

Substituting in the energy equation (eqn (4));

$$\rho C_p\frac{\partial T}{\partial t}=\frac{k}{r}\frac{\partial}{\partial r}\left(r\frac{\partial T}{\partial r}\right)+\eta_0\left[\frac{r}{2\eta_0}\left(\frac{\partial P}{\partial z}\right)\right]^{(n+1)/n} \tag{14}$$

Equations (13) and (14) were solved using a finite difference method to find the temperature profile and pressure drop in the molten zone.

To simplify the calculation, thermal conductivity and density were treated as constant with temperature. A simple method was used to incorporate the enthalpy of fusion of the polymer ΔH_m, which acts as a heat source in nodes which lie within the melting region [8]. The enthalpy was added to the specific heat change in the melting region ΔT_m:

$$\Delta C_p = \Delta H_m / \Delta T_m \quad (15a)$$

$$\bar{C}_p = C_p + \Delta C_p \quad (15b)$$

This approach was used for both filled and unfilled polymer.

As shown in eqn (11) $\partial P/\partial Z$ is a function of viscosity which varies with temperature. An average viscosity was used in the initial calculation and the implications of this simplification are investigated quantitatively below. The pressure drop, the internal heating and the temperature distribution can thus be calculated. When no flow takes place ($Q = 0$), for example during the dead time, the pressure is zero and eqn (14) reflects passive heat transfer. During oscillation, if the heat loss is larger than the heat generated by shear flow, the material cools and the dimensions of the molten channel decrease. As a result, the pressure needed to maintain the displaced volume increases. The criterion for the cessation of flow is that the pressure drop becomes equal to the set pressure on material in the oscillating valve. Thereafter the passive heat transfer calculation was used for the temperature distribution. The values of the parameters used in the calculation and their sources [8, 13] are given in Table 1.

The finite difference calculations for passive cooling were checked against the analytical model for unsteady state heat flow [8]. The calculations for active solidification (during reciprocating flow) were tested by putting the term $(\partial V_z/\partial r)$ in eqn (4) equal to zero. The temperature gradients thus deduced correspond to the passive situation. A further check was made by estimating the temperature change with $\Delta T = \Delta P/\rho C_p$. This represents an approximation for the heat generated in steady shear flow in a capillary [14]. Finally and decisively, the model was tested by comparing calculated freeze-off times with those measured experimentally during injection moulding.

Table 1. Values of material properties used in the calculations and their sources

Properties	Polypropylene	Ceramic mixture	Source reference
c_p/J kg^{-1} K^{-1}	1710	1012	13
ρ/kg m^{-3}	910	2740	13
k/W m^{-1} K^{-1}	0.15	1.5	13
ΔH_m/J kg^{-1}	87,000	5700	13
h/W m^{-2} K^{-1}	1500	1500	8
η_0/Pa s	7901	1561	this work
n	0.43	0.49	this work
ΔT_m/K	20	20	13

3. EXPERIMENTAL PROCEDURE

Polypropylene mouldings were made using grade HW1925 (ICI Welwyn, U.K.) and ceramic suspensions were prepared from fine alumina (grade RA6, Alcan Chemicals, Gerrards Cross, U.K.) with an average particle size of 0.9 μm in an organic vehicle consisting of isotactic polypropylene (grade GY545M, ICI, Welwyn, U.K.), atactic polypropylene (grade MF70, APP Chemicals, Salop, U.K.) and stearic acid (grade GPR, BDH Chemicals, Poole, U.K.) in the weight ratios 4:4:1. The mixing was carried out using an intermeshing co-rotating twin screw extruder (Model TS40 Betol Machinery, Luton, U.K.) using a procedure fully described elsewhere [15]. Samples of about 15 g were ashed to check the ceramic content. Apparent viscosities of both materials were measured using a Davenport Capillary Rheometer with a die of diameter 2 mm and length 40 mm at a range of shear rate from 5 s^{-1} to 725 s^{-1}. The temperature range of 160 to 220°C was explored. Differential scanning calorimetry was used to find the enthalpies of melting and the temperatures of onset and completion of solidification.

Injection moulding was carried out on a Demag D150 NCIII-K machine (Mannesmann Demag, Kunststofftechnik, Schwaig, Germany) fitted with an hydraulically-activated double-gated modulated pressure device described elsewhere [2]. The oscillating pistons had a diameter of 10 mm and a stroke of 70 mm. The nozzle diameters and lengths were 6 mm and 110 mm, respectively. The barrel temperatures for all mouldings were 180–200–210–210°C feed to nozzle. The injection and hold pressures were set at 28 and 14 MPa respectively. Position trip was used to initiate oscillation.

The mould cavity was an end-gated 15 mm × 10 mm rectangular section bar of length 70 mm. Two sprues, each with a 2° taper and length 90 mm were used. Sprues A and B had minimum diameters of 8 mm and 4 mm respectively. The cross sections of runners for sprues A and B were trapezoidal with dimensions 8.8 mm × 6.1 mm × 7 mm depth and 7.8 mm × 5.6 mm × 5.8 mm depth, respectively. Only sprue B was used for unfilled polypropylene. The mould cavity pressure was measured with a 4 mm pin acting on a 4450 N force transducer. The mould temperature was controlled by a 3 kw thermostated water circulation unit (UTAC Engineering Ltd, Dorset, U.K.).

4. RESULTS AND DISCUSSION

4.1. *Apparent viscosity measurements*

Flow in the rheometer could be achieved above 175°C for the polypropylene and above 165°C for the ceramic suspensions. In the temperature ranges given

Table 2. Relation between apparent viscosities and temperature

Material	Temperature (°C)	η_0 (Pa s)	n	R^*
Polypropylene	175	8849	0.43	0.995
	180	8630	0.43	0.995
	190	7901	0.43	0.997
	200	6333	0.46	0.995
	210	6182	0.45	0.998
Ceramic suspension	165	47,655	0.23	0.986
	170	7353	0.47	0.987
	175	5748	0.43	0.992
	180	4732	0.54	0.987
	190	2620	0.49	0.996
	200	2443	0.46	0.998
	210	2048	0.50	0.999
	220	1755	0.47	0.990

* Regression coefficient.

in Table 2, the relationship between shear stress and shear rate was linear on logarithmic axes suggesting that the material can be treated in this range as a power law fluid for which:

$$\tau = \eta_0 \dot{\gamma}^n \tag{16}$$

The flow behaviour index n, was nearly independent of temperature in this region. The flow behaviour index of the suspension was higher than that for unfilled polypropylene; an effect attributable to the rearrangement of particles in shear flow (16). For the unfilled polymer and the ceramic suspensions, the temperatures at which flow effectively ceased due to crystallization were 175°C and 165°C and above these temperatures the viscosity changed very slightly with temperature as shown in Fig. 3.

4.2. *Passive cooling*

The time at which the narrowest end of the sprue freezes can be compared with the time at which cavity pressure begins to decay for conventional mouldings made without oscillating pressure. For a semi-crystalline polymer, a loose correlation is expected because the cavity pressure falls when the volumetric shrinkage rate of the cavity contents just exceeds the flow rate in the sprue needed to compensate for shrinkage. This flow rate is vanishingly small compared to the flow rates at which oscillating pressures ceases to be effective, and the problem has been discussed in detail by Hunt *et al.* [17].

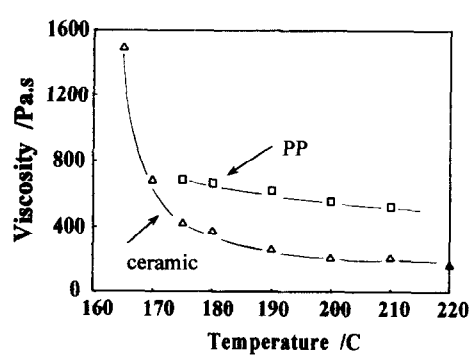

Fig. 3. Apparent viscosity of polypropylene and the ceramic suspension at a shear rate of 90 s^{-1}.

The solidification times calculated using eqn (2) are compared with cavity pressure decay times in Table 3. Very small flow rates are needed to compensate for shrinkage and so the cavity pressure decay time in conventional moulding correlates with the time at which the centre of the sprue reaches the dilatometric softening point, namely 142°C for polypropylene and 146°C for the ceramic suspension. These temperatures are lower than those deduced from rheometry for application to oscillating pressure conditions, namely 175°C and 165°C respectively and this accounts for the longer time observed for cavity pressure decay. This comparison neglects axial heat flow from the nozzle, undercooling and the effect of pressure on crystalline melting point and viscosity. Thus even for conventional injection moulding it is not a simple matter to predict accurately the point at which flow ceases and this should be held in mind when judging the accuracy of the model for oscillating pressure moulding.

4.3. *Modulated pressure moulding*

Oscillating pressure injection mouldings were then produced using the conditions shown in Table 4. The penultimate column shows the times at which the pistons ceased to displace their contents and these times are compared with values calculated from the numerical model. Bulk flow effectively ceases when the molten zone is about 1 mm in diameter giving rise to a demanded pressure which exceeds the set pressure amplitude.

During the first few oscillations, the displacement time for both materials was about 1 s, after which it settled to 2 s. The first five rows of Table 4 which refer to unfilled polypropylene therefore show the effect of increasing the dead time. For cycle times less than 7.6 s, the moulding can be kept molten indefinitely. As the cycle time is extended further, the quasi-steady state is lost and solidification time falls rapidly as predicted by the model. The agreement between experimental and calculated times in Table 4 is good for both materials. The main error is in the time for flow to cease in polypropylene mouldings and this is accounted for by the underestimation of the molten zone diameter throughout the runner and sprue system which arose in the following way.

A mould temperature of 40°C and a sprue of 4 mm dia. were used for moulding unfilled polypropylene but these conditions did not allow reciprocating flow to be achieved for the ceramic suspension which has a higher thermal diffusivity. For this, the mould temperature was set to 80°C and the 8 mm dia. sprue was used with the larger runner.

Table 3. Solidification time during conventional injection moulding (injection temperature 210°C)

Material	Sprue diameter/ mm	Mould temperature/ °C	Injection and hold pressure/ MPa	Cavity pressure decay time/s Measured*	Calculated
Polypropylene	4	40	60	24	14
	4	40	80	18	14
	4	40	110	20	14
Ceramic suspension	4	80	60	4	4
	8	80	60	11	10.5

* Average of 5 mouldings deduced from cavity pressure decay.

Table 4. Solidification time under various moulding conditions (mould temperature was 40°C and 80°C for polypropylene and ceramic mixture respectively)

Material	Sprue dia./mm	Osc. pressure/MPa	Cycle time/s	Time at which flow ceases/s Expt.	Calc.
Polypropylene	4	165	6	∞	∞
	4	165	7	∞	∞
	4	165	7.6	∞	∞
	4	165	8	110	18
Ceramic suspension	4	165	3	4–8	6
	4	165	4	4–8	6
	8	165	4	18–22	25
	8	110	4	16	15

A simplication in the model is that the molten core of the runner system is treated as a cylinder of length equal to the runner length and diameter equal to the smallest section. Figures 4(a) and (b) show the isotherms for the trapezoidal section runners which were treated, for geometrical simplification, as rectangular sections with width at half height. The molten zone in these sections gradually developed an ellipsoidal section and this justifies the approximation of taking the molten flowing sections as cylindrical for the purpose of calculating the heat dissipated in viscous flow in the feeder during oscillation.

Figure 5 shows the diameter of the molten zone in the narrowest section of the conical sprue as a function of time. By comparing Fig. 4(b) with curve "b" in Fig. 5, it can be seen that the diameters of the molten zone in the runners converge with those for the sprue in the case of the ceramic moulding. In fact, the cross sectional area of the large runner was equal to that of the small end of the sprue (50 mm^2). The natural cooling time for a mould temperature of 80°C was 7 s for the runner compared with 8 s for the sprue; a difference caused by geometry.

In the case of the polypropylene mouldings on the other hand, for which the small (4 mm dia.) sprue was employed, there is a large difference in section along the feeder system. Thus comparing Fig. 4(a) with curve "a" in Fig. 5, it can be seen that treating the entire feeder system as a cylinder with radius corresponding to the smallest section of the sprue can be expected to significantly overestimate the pressure needed to maintain flow and hence underestimate the solidification time. The 4 mm dia. sprue had a much smaller cross sectional area (13 mm^2) compared with the area of the small runner (39 mm^2).

In assessing the disparity in Table 4 between the experimental solidification time of 110 s and the calculated time of 18 s for polypropylene, it is interesting arbitrarily to change the diameter of the sprue in the calculation. When the diameter was increased to 7 mm, flow was predicted to cease after 40 s rather than 18 s and when the diameter was 8 mm, stable oscillation was predicted. The "effective" diameter along the length of the runner giving rise to 110 s thus lies between these values of diameter and the sensitivity to the diameter of the runner system can be clearly seen. This is the parameter which is very costly to change in trial and error experimental work and highlights the need for a simple predictive model.

When the molten zone diameter in the bar was compared with that in the sprue and runners, it was evident that its diameter was much larger and hence shear rate in the bar is lower. For example, in polypropylene mouldings, the elliptical molten zone in the runner after 20 s had principal diameters 1.7×2.2 mm compared to those for the bar 6.2×11 mm. In ceramic

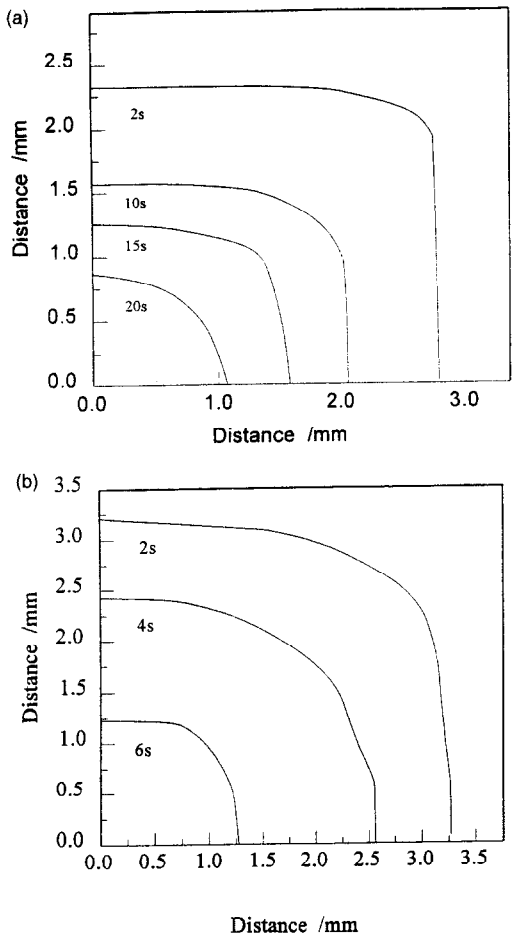

Fig. 4. Loci of the solid–liquid interface in the quarter section of the trapezoidal runner treated as a rectangle having width at half height for (a) polypropylene; mould temperature 40°C and actual runner 7.8 mm × 5.6 mm × 5.8 mm thick and (b) ceramic suspension; mould temperature 80°C and actual runner 8.8 mm × 6.1 mm × 7.0 mm thick.

mouldings after 6 s the principal diameters of the runner were 2.4 × 2.5 mm compared to 6.5 × 10.5 mm for the bar. The length of the bar is much shorter (70 mm) than that of the feeder system (280 mm). It is therefore justifiable to treat the molten channel as a cylinder having a length corresponding to the total length of the sprues and runners but omitting the path length of the rectangular bar.

The model is also very successful in predicting the frequency threshold below which the flow is unstable with high accuracy even for polypropylene. Rows 4 and 5 of Table 4 show that the steady state is reached for a cycle time between 7.6 and 8 s. In a similar way, it is shown both experimentally and by calculation that it is not possible to generate stable oscillation in the ceramic suspension with a maximum oscillation pressure of 165 MPa. Figure 6 shows the relevant cooling curves. The centre temperature is maintained above the solidification temperature for 26 s but during this time the pressure needed to maintain flow consistently rises as the radius of the molten zone decreases. When the maximum set pressure is reached,

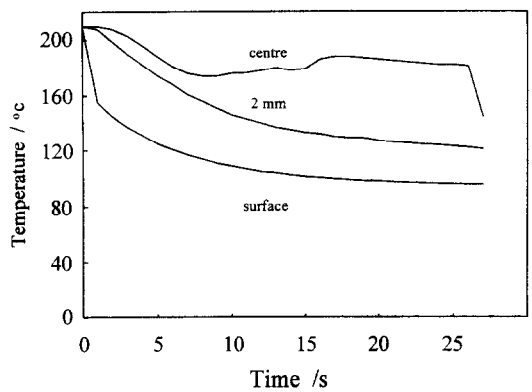

Fig. 6. Cooling curves for the centre, surface and intermediate nodes of an 8 mm dia. cylinder of ceramic suspension subjected to oscillating pressure at a cycle time of 4 s in a mould at 80°C.

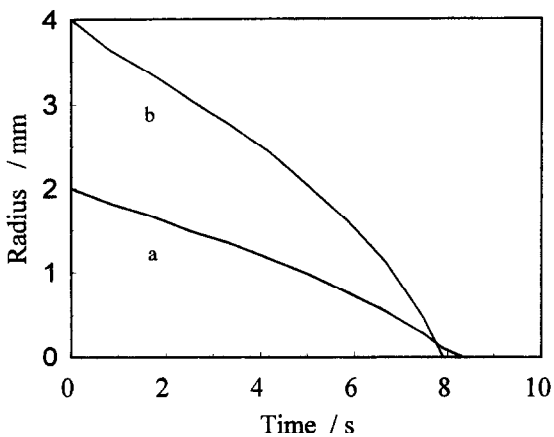

Fig. 5. Radius of the molten zone in the sprue as a function of time for (a) polypropylene; mould temperature 40°C and sprue diameter 4 mm (b) ceramic suspension; mould temperature 80°C and sprue diameter 8 mm.

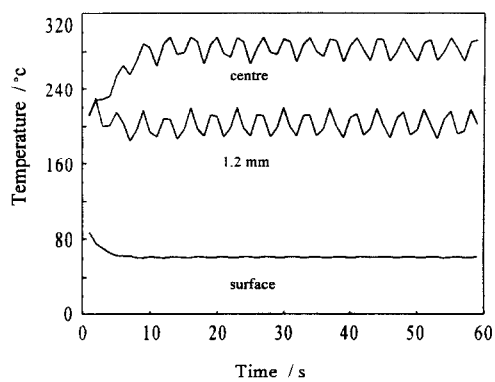

Fig. 7. Cooling curves for the centre, surface and an intermediate node for a 4 mm dia. sprue for polypropylene subjected to oscillation at a cycle time of 7 s (mould temperature 40°C).

the flow promptly ceases. The temperature of the centre thereafter follows the natural cooling curve. The experimental time at which this occurred was between 18 and 22 s. The accuracy of this prediction compared with the accuracy for polypropylene mouldings is because the diameter of the molten zone was more uniform along the length of the feeder system.

The temperatures in the feeder at various points were calculated for modulated pressure polypropylene mouldings and show the generation of stable temperatures (Fig. 7). For the solid zone and the molten zone during the "dead-time", the velocity gradient is zero, and no shear heat is generated so the passive heat transfer calculation was used. Figure 7 shows cooling curves for the centre, the radial shell at $r = 1.2$ mm and the surface for polypropylene at a cycle time of 7 s. After about 14 s, the average temperature in the molten zone is stable and the material in the circuit can be kept molten indefinitely. This agrees with experiment (Table 3, row 2). The centre temperature is predicted to rise to nearly 300°C. The stable state is not helpful for orientation of the centre of the moulding which requires a steadily decreasing radius in which shear flow causes alignment. In fact, the temperature excess calculated by this method is exaggerated because the melt exchanges heat with the cooler nozzle and piston chamber as discussed in Section 5.

A high temperature gradient should also prevail in the moulding because of forced convective flow even though negligible heat is generated therein. The polypropylene mouldings made with long oscillation periods contained internal shrinkage voids which could be prevented by a high packing pressure after oscillation. The nucleation and growth of such a void was observed by opening the clamp after oscillation for 600 s. The void nucleated without the development of sink marks on the surface of the moulding. This indicates that the surface of the moulding was cold, despite an internal molten zone and supports the existence of steep temperature gradients predicted by Fig. 7. In conventional moulding, such a steep temperature gradient cannot be obtained and sinking deformation accompanies voiding. Sinking deformation can only occur when the surface layers are close to the solidification temperature and the cavity pressure has collapsed.

When a 4 mm dia. sprue was used, the solidification time for ceramic mouldings was much shorter than that for polymer mouldings, as shown in Tables 3 and 4. This indicates the sensitivity of the process to thermal properties of the fluid and shows that no significant extension to solidification time compared with the conventional injection moulding could be achieved with the small sprue as shown by experiment and calculation. The solidification time could be extended by fitting an 8 mm dia. sprue (Tables 3 and 4). This also illustrates the sensitivity of the process to the physical dimensions of the circuit and indicates that mould tool design must take account of the thermal properties of the moulding material.

Figure 8 illustrates the effect of mould temperature. It shows how the radius of the molten zone falls and the demanded pressure rises for the ceramic suspension moulded with an oscillation period of 4 s in a sprue of 8 mm dia. Figure 8(a) indicates that the demanded pressure reaches the set pressure of 165 MPa after 10 s if the mould temperature is 20°C but after 26 s if the mould temperature is increased to 80°C (Fig. 8(b)). When the mould temperature is increased, the temperature gradient across the moulding is reduced and heat lost to the mould wall is less. If other variables remain unchanged, this results in a higher excess temperature in the molten core. It follows that a higher mould temperature allows a lower frequency to prolong solidification time.

Figure 9 shows sections of polypropylene from the sprue, runner and mould cavity sections, revealing this history of solidification rather in the way that dendrochronologists have access to the climatic record. The dark central regions represent shrinkage porosity caused by cooling the melt from a temperature in excess of the injection temperature without an applied pressure after oscillation has terminated. The uniformly absorbing central region is unoriented polymer which has undergone passive solidification after oscillation ceased and any orientation present has been annealed. These micrographs confirm that

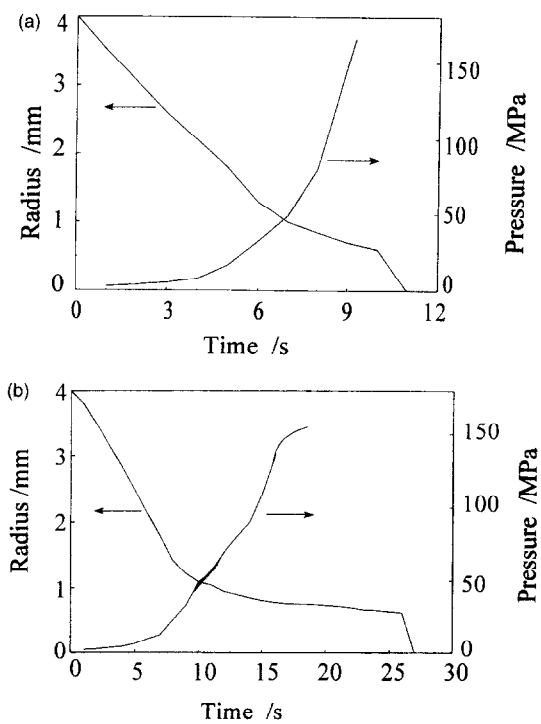

Fig. 8. Radius of the molten zone and demanded pressure for ceramic suspension oscillated at a cycle time of 4 s in a sprue of 8 mm dia. and mould temperature (a) 20°C, (b) 80°C.

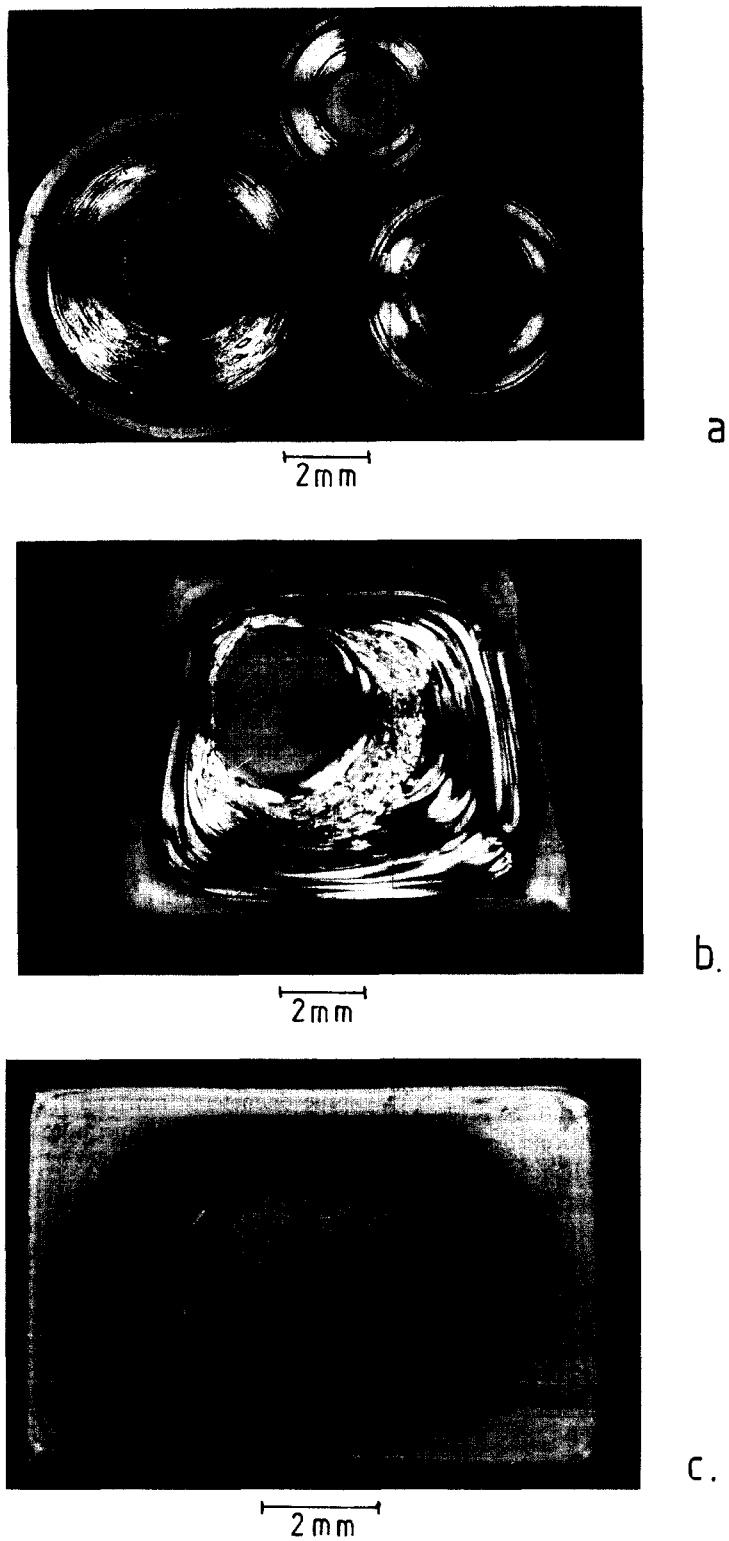

Fig. 9. Polished cross sections in polarized transmitted light of (a) sprue, (b) runner and (c) cavity after 600 s oscillation. (Mould temperature 40°C; cycle time 7 s.)

the molten zone diameter along much of the conical sprue is nearly the same as that in the trapezoidal runner which was the assumption used in the numerical model. However, at the wide end of this small sprue, the molten zone is significantly greater which is the source of the error in predicting the freeze-off time for polypropylene (Table 4, row 4).

The cross sectional area of the molten zone in the mould cavity (Fig. 9(b)) is much greater and justifies not including it as a region where shear induced heating is sourced. The rectangular bar section shows a series of concentrical layers which are made visible by slight differences in refractive index of oriented and unoriented material. Although the moulding has been subjected to about 170 displacements, only the first 13 are recorded as discrete visible lines in the microstructure. Near the centre, the lines converge because so much heat is generated that solidification cannot continue under modulated pressure conditions and the quasi-steady state is reached.

5. ASSESSMENT OF ERROR

The main source of error is the underestimation of molten zone diameter, resulting from taking the smallest diameter of the runner system as the cylindrical radius. Its consequences for the polypropylene mouldings made with a smaller sprue have been discussed. Thus in any moulding configuration in which the feeding system has widely differing cross sections, the choice of an effective diameter and length for the part of the system which solidifies first is crucial.

The calculations also neglect the heat exchanged between the displaced melt and heated nozzle and cylinder. In the case of polypropylene, where oscillation causes a temperature excess, this transfer would result in cooling of the reciprocating liquid. In the ceramic suspensions, no temperature excess is expected and a heating effect would occur during entry and storage in the nozzle and cylinder. These heat transfers were estimated using eqn (2) by changing the boundary temperature condition. During displacement of the melt from the mould to the nozzle, laminar flow conditions do not prevail and mixing is expected so the average temperature of the melt is needed. This can be calculated from

$$T = \frac{\Sigma T_i V_i}{\Sigma V_i} = \frac{\Sigma T_i 2\pi r_i \Delta r}{\Sigma 2\pi r_i \Delta r} \qquad (17)$$

where subscript "i" denotes the radial node number. Table 5 shows that these heat transfers do affect the average melt temperature. If the material flows into the nozzle at 320°C (a 110°C excess over the injection temperature) and stays in the nozzle/cylinder assembly for half the cycle time, the temperature drop, due to cooling in the nozzle and cylinder, will be 24°C. The temperature drop would be about 30% of the temperature change seen on each cycle in Fig. 7. The actual temperature rise during oscillation will therefore be less than that predicted.

For the ceramic suspension, no temperature rise is seen during oscillation and all nodes show cooling. At a stage when the material flows back into the nozzle at 180°C, the average temperature rise will be 6°C after one second. The higher thermal diffusivity of the ceramic suspension means that the acquisition of heat from the pumping cylinders and nozzle effectively prolongs solidification. A full analysis of the forced convective heat transfer would need to accommodate the variation in displacement distance as well as displaced volume and hence would require a knowledge of the molten volume in the cavity as a function of time.

Since viscosity is a function of temperature, the use of a fixed viscosity in the calculations is a source of inaccuracy. An increase in viscosity would increase the heat source and the pressure required for flow. These effects tend to cancel each other. The influence of viscosity was tested in the model for polypropylene in a mould at 40°C and a cycle time of 8 s. When the lower viscosity appropriate to 210°C was used instead of that prevailing at 190°C, the solidification time was extended but only by about 3 s. Similarly for the ceramic suspension, when the lower viscosity appropriate to 190°C was used instead of that prevailing at 175°C, the solidification time was extended by about 3 s.

The effect of flow rate on the temperature of the ceramic injection moulding suspension is shown in Fig. 10. Figure 10(a) shows the centre temperature for polypropylene with a mould temperature 40°C, cycle time 7 s and 4 mm dia. sprue with a normal and reduced flow rate. The temperature in the centre of the sprue decreased by 15°C in the stable regime as a result of this simulated error. The corresponding comparison for the ceramic suspension is shown in Fig. 10(b). The mould temperature was 80°C, the sprue diameter 8 mm and the cycle time 4 s. For the first 15 s the temperature change is negligible. Thereafter a lowered flow rate prevents the supplied heat from balancing that lost to the mould wall and the material in the sprue quickly cools. Thus a variation or error in flow rate has the effect of reducing the predicted finishing time from 26 s to 18 s. The experimental values were 18–22 s.

6. CONCLUSIONS

A numerical computer model has been developed to address the heat balance during double-gated modulated pressure injection moulding in order that the principal processing variables and their effects can be found. The sources of error have been assessed quantitatively. The model accurately predicts the conditions above which stable oscillating flow can be prolonged indefinitely for low thermal conductivity materials. It predicts that, with the available pressures, stable oscillation cannot be achieved for the high ther-

Table 5. Heating or cooling in the nozzle and oscillation cylinder (nozzle and oscillation cylinder temperature 210°C)

Material	Diameter of residence cylinder* (mm)	Material† temperature (°C)	Time‡ (s)	Average† temperature after t s (°C)
Polypropylene	6	180	2	187
	6	180	3	189
	10	180	2	185
	10	180	3	186
	6	320	2	296
	10	320	2	305
	6	260	2	250
	10	260	2	254
Ceramic suspension	6	180	1	186
	6	180	2	190
	10	180	1	183
	10	180	2	186

* Nozzle diameter 6 mm, oscillation cylinder diameter 10 mm.
† Temperature of material which flows back to the nozzle or oscillation cylinder.
‡ Time for which the material stays inside the nozzle or cylinder.

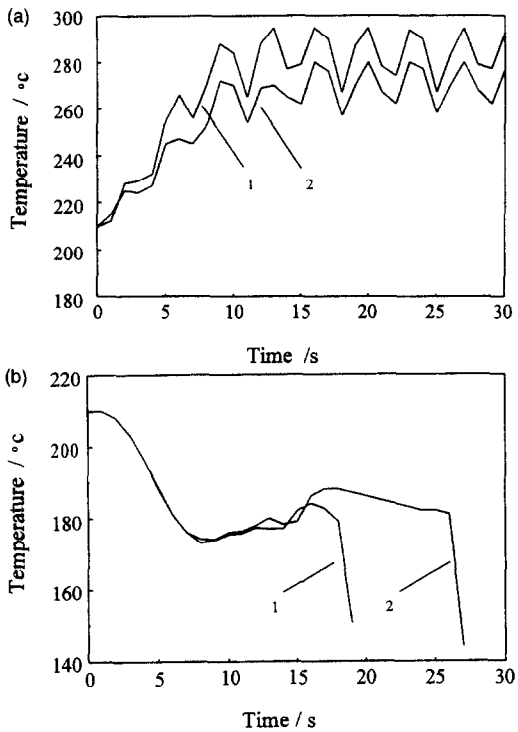

Fig. 10. Centre temperature (a) for polypropylene with a mould temperature 40°C, cycle time 7 s and 4 mm dia. sprue for (1) full flow rate and (2) 90% flow rate; (b) for ceramic suspension with a mould temperature 80°C, cycle time 4 s and 8 mm dia. sprue for (1) full flow and (2) 90% flow.

mal conductivity material. It also predicts the time at which flow ceases for the higher thermal conductivity ceramic suspension.

For low thermal conductivity materials under conditions of high oscillation frequency and high preset pressure, the model predicts a significant temperature increase in the middle of the mould cavity. The temperature excess can be reduced by using a large sprue or by increasing the "dead time". For powder injection moulding suspensions which have high thermal conductivity, the oscillating flow can be extended by using a higher frequency, a larger sprue and higher mould temperature.

The model shows how a systematic selection of moulding parameters can be used to optimize the process. The main source of error was encountered in the prediction of flowing time for the unfilled polymer and this can be attributed to the assumption that the entire length of the molten channel has the diameter of the molten zone at the narrow end of the sprue. While much refinement of the model is possible, in its present form it predicts the high sensitivity of the process to frequency, sprue size, mould temperature and thermal properties of the material.

Acknowledgements—The authors are grateful to EPSRC for supporting this work under Grant No. GR/H97123, to Dr P. Allan and Dr J. Gibson for the help in the injection moulding work and to Mrs K. Goddard for typing the manuscript.

REFERENCES

1. Folkes, M. J., In *Short Fibre Reinforced Thermoplastics*, M. J. Bevis (ed.) Research Studies Press, Chichester, U.K., 1982, pp. 101–109.
2. Allan, P. S. and Bevis, M. J., Multiple live feed injection moulding. *Plast. Rubb. Proc. Appln*, 1987, **7**, 3–10.
3. Allan, P. S. and Bevis, M. J., Development and application of multiple live feed moulding for the management of fibres in moulded parts. *Composites Manufacturing*, 1990, **1**, 79–84.
4. Kalay, G., Allan, P. S. and Bevis, M. J., Microstructure

and physical property control of injection moulded polypropylene. *Plast. Rubb. and Comp. Proc. Appln*, 1995, **23,** 71–85.
5. Wang, L., Allan, P. and Bevis, M. J., Enhancement of internal weldline strength in thermotropic liquid crystal polymer mouldings. *Plast. Rubb. and Comp. Proc. Appln*, 1995, **23,** 139–150.
6. Pinwill, I. E., Ahmed, F., Allan, P. S. and Bevis, M. J., Application of shear controlled orientation technology to powder injection moulding. *Powder Metall.*, 1992, **35,** 107–112.
7. Allan, P. S. and Bevis, M. J., Shear controlled orientation in extrusion. *Plast., Rubb. and Comp. Proc. Appln*, 1991, **16,** 133–137.
8. Zhang, T. and Evans, J. R. G., The calculation of temperature distributions in ceramic injection moulding *J. Amer. Ceram. Soc.*, 1992, **75,** 2260–2267.
9. Zhang, T. and Evans, J. R. G., Computation of volume flow in modulated pressure injection moulding. *Ceramics International*, 1993, **19,** 367–373.
10. van Krevelin, D. W., *Properties of Polymers*. Elsevier, Oxford, U.K., 1976, pp. 347–348.
11. Croft, D. R. and Lilley, D. G., Heat transfer calculations using finite difference equations, 1977. Applied Science Publishers, London, pp. 77–83.
12. Lenk, R. S., *Polymer Rheology*. Applied Science Publishers, 1978, London, p. 78
13. Zhang, T., Evans, J. R. G. and Dutta, K. K., Thermal properties of ceramic injection moulding suspensions in the liquid and solid state. *J. Euro. Ceram. Soc.*, 1989, **5,** 303–309.
14. Fenner, R. T., *Principles of Polymer Processing*. Macmillan Press, London, 1979, pp. 23–29.
15. Zhang, T. and Evans, J. R. G., Predicting the viscosity of ceramic injection moulding suspensions. *J. Euro. Ceram. Soc.*, 1989, **5,** 165–172.
16. Casson, N., A flow equation for pigment-oil suspensions of the printing-ink type. In *Rheology of Dispersive Systems*, C. C. Mill (ed.). Pergamon, Oxford, 1959, pp. 84–104.
17. Hunt, K. N., Evans, J. R. G. and Woodthorpe, J., Computer modelling of the origin of defects in ceramic injection moulding III; Sprue closure. *J. Mater. Sci.*, 1991, **26,** 2143–2149.